PHYSICAL REVIEW B VOLUME 23, NUMBER 10 15 MAY 1981

Electronic structure of pseudobinary semiconductor alloys $Al_xGa_{1-x}As$, GaP_xAs_{1-x}, and $Ga_xIn_{1-x}P$

A.-B. Chen
Department of Physics, Auburn University, Auburn, Alabama 36849

A. Sher
SRI International, Menlo Park, California 94025

(Received 23 October 1980; revised manuscript received 29 December 1980)

A method for calculating detailed electronic properties of the pseudobinary III-V compound semiconductor alloys is presented. The technique begins with realistic band structures obtained for the constituent compounds by fitting the band-gap symmetry-point energies and effective masses to experimental data, where they are available, and to more sophisticated theoretical results. Then the coherent-potential approximation is used to calculate the alloy band structures and scattering rates. Detailed comparisons between the theoretical predictions and experimental data for three alloys $Al_xGa_{1-x}As$, GaP_xAs_{1-x}, and $Ga_xIn_{1-x}P$ demonstrate the quantitative nature of the method. Bowing parameters for the Γ, X, and L gaps and the direct-to-indirect band-gap crossover concentrations are all predicted to within the present degree of experimental certainty.

I. INTRODUCTION

Studies of the electronic structure of substitutional semiconductor alloys, along with their closely related device applications, have become an active part of semiconductor physics. Although a theory capable of interpolating alloy band structures between those of the pure constituent compounds is desirable, no sufficiently detailed method to accomplish this end currently exists. Many prior theories[1-5] have been designed to predict only trends of specific band quantities, such as the band gaps[1-4] and the effective masses[5] at band edges.

The virtual-crystal approximation (VCA) is essentially the only method that has been used for detailed alloy band-structure calculations. VCA treats an alloy as a perfectly periodic crystal with an average potential at each sublattice site and does not include in lowest order the effects of aperiodic fluctuations in the crystal potentials. When the aperiodic part of the potential is sufficiently small, perturbation theory can be applied to the VCA results to account for some disorder-induced effects.[6,7] Even in the few cases in which attempts were made to treat realistic systems, the results were not completely satisfactory.[7] For stronger scattering cases, Monte Carlo methods[8] have been used to treat transport properties. There is no satisfactory theory that is based on a well defined set of potentials and predicts a wide range of phenomena, such as the alloy concentration variation of band energies, effective masses, and mobilities. However, the coherent-potential approximation (CPA),[9-11] in which both stronger and weak scattering potentials in concentrated alloys can be treated, offers the prospect of predicting the outcomes of a wide range of experiments. We report the results of such a CPA calculation in this paper.

In a previous paper[11] (referred to henceforth as I), we reviewed the application[10] of CPA to semiconductor alloys and applied it to the valence bands of III–V compound alloys. The bond-orbital model (BOM),[12,13] which is only suitable for the valence bands, was employed in that study. Here the more accurate band-calculation method introduced by Kane[14] and Chadi,[15] which takes better account of the long-range interactions and consequently applies well to both the conduction and valence bands, is cast into the form of a CPA calculation.

In seeking a practical alloy interpolation method, we have set two requirements. First, the underlying band-structure method must be capable of producing quantitatively accurate results for the pure compounds. Second, the method must be simple enough so efficient numerical alloy calculations can be implemented and many cases tried. With these requirements in mind, in a separate paper[16] (denoted II) we made a systematic study of the Hamiltonian matrix elements and band structures of the III–V compounds using simple Gaussian orbitals and pseudopotentials. Accurate results for both the valence and conduction bands were obtained using a universal basis set, which is identical in crystal units (cu) for all the III–V compounds. Furthermore, we introduced a technique that was designed to add small corrections to the Hamiltonian. These corrections were selected so the important symmetry-point band energies and effective masses were fitted to experimental or more sophisticated theoretical results.

To facilitate the CPA calculation, the basis states used in II are here recast into orthonormal bonding and antibonding basis functions. If the alloy calculation is attempted in a highly nonorthogonal basis set, the correlations in the higher-order terms of the multiple scatterind expansion are so strong that CPA fails. However, this problem is not present when the orthogonal basis set associated with the bonds is used. The Hamiltonian matrix studied in I and II, where we demonstrated that the main differences from one compound to another reside in the diagonal elements, justifies the assumption that the most important alloy disorder stems from variations in the local bonding and antibonding energies. Given this result, the alloy calculation can be carried out easily in a manner similar to that used in I.

Once the CPA self-energies are obtained, detailed band energies, effective masses, and alloy scattering lifetimes can be calculated. Since relativistic effects are not included in the present formalism, we have chosen for initial application of the method the three well studied alloys $Al_xGa_{1-x}As$, GaP_xAs_{1-x}, and $Ga_xIn_{1-x}P$ for which the relativistic effects are not too important. Comparison of our results with experiments shows that the calculations agree with relevant data. Moreover, the detailed results also predict the behavior of some quantities for which the present experimental situation is uncertain, e.g., the concentration variation of the L_{1c} energies.

The remainder of this paper is arranged in the following order. Section II describes the calculational procedure. Section III presents an analysis of the input quantities and the resulting band structures of the pure constituent compounds. The alloy band structures and their comparison with experimental results are presented in Sec. IV. The final section is devoted to the principal conclusions and a summary.

II. CALCULATIONAL PROCEDURE

A procedure using simple Gaussian orbitals and pseudopotentials to calculate the band energies of III–V compound, zinc-blende structured semiconductors has been presented in II.[16] This method will now be extended to a CPA calculation for alloys. Because the details have already been published, our presentation of the underlying method will be brief.

A Gaussian orbital of type α (α is either an s, p_x, p_y, or p_z orbital) for the jth sublattice (j is the anion or the cation sublattice) in the $\vec{l}$th cell ($\vec{l}$ is a fcc lattice vector) is denoted by $|\vec{l}j\alpha\rangle$. The Bloch basis constucted from $|\vec{l}j\alpha\rangle$ is denoted as $|\vec{k}j\alpha\rangle$. In the basis set $\{|\vec{k}j\alpha\rangle\}$, the overlap matrix $S(\vec{k})$ and the Hamiltonian matrix $H_0(\vec{k})$ derived from empirical pseudopotentials can then be calculated.[14-16] To establish accurately certain important band-structure features adjacent to the gap, an extra 8×8 Hamiltonian matrix $H_1(\vec{k})$ is added to $H_0(\vec{k})$.[16] This extra Hamiltonian matrix simulates the effects of nonlocal pseudopotentials and an expanded orbital set. Finally, an energy shift $\Delta\epsilon$ is included that aligns the absolute energies with respect to the vacuum to the measured values. Thus, the Hamiltonian matrix in the basis $\{|\vec{k}j\alpha\rangle\}$ contains three terms,

$$H(\vec{k}) = H_0(\vec{k}) + H_1(\vec{k}) + \Delta\epsilon S(\vec{k}) . \tag{1}$$

The band energies $\epsilon_n(k)$ are obtained from the equation

$$\det[H(\vec{k}) - \epsilon_n(\vec{k}) S(\vec{k})] = 0 . \tag{2}$$

In II it is demonstrated that it is possible to cast the problem in a basis set of Gaussian orbitals in which, in crystal units, the same exponential factors apply for all III-V compounds In this universal basis, the overlap matrix $S(\vec{k})$ and the kinetic-energy matrix in cu are the same for every compound. The band structures resulting from this method reproduce the results of elaborate band calculations to within a few percent throughout the Brillouin zone.

The Gaussian orbitals centered on different atoms are not orthogonal. However, it is essential to formulate the CPA theory in terms of an orthonormal basis. One way to accomplish this is to start with the Wannier basis,

$$\left| W_n(\vec{l}) \right\rangle = \frac{1}{\sqrt{N}} \sum_{\vec{k}} e^{-i\vec{k}\cdot\vec{l}} \left| \psi_{n\vec{k}} \right\rangle , \tag{3}$$

where N is the number of anions or cations in the crystal, and $|\psi_{n\vec{k}}\rangle$ is an orthonormal energy eigenstate

$$\hat{H}|\psi_{n\vec{k}}\rangle = \epsilon_n(\vec{k})|\psi_{n\vec{k}}\rangle . \tag{4}$$

Here $\hat{H}$ is the operator corresponding to $H(\vec{k})$ in Eq. (1) expressed in an orthonormal basis set. We note that $|\psi_{n\vec{k}}\rangle$ can be constructed from the set $\{|\vec{k}j\alpha\rangle\}$ after the generalized eigenvalue problem Eq. (2) is solved. The Wannier basis set is also orthonormal,

$$\langle W_n(\vec{l})|W_{n'}(\vec{l}')\rangle = \delta_{nn'}\delta_{\vec{l}\vec{l}'} . \tag{5}$$

A natural local basis for the tetrahedrally bonded materials is the set of bonding orbitals $|b_i(\vec{l})\rangle$ and antibonding orbitals $|a_i(\vec{l})\rangle$, $i = 1, \ldots, 4$.[17] If we choose $\vec{l}$ to be the displacements of the atoms on one sublattice, the four orbitals $|b_i(\vec{l})\rangle$, $i = 1, \ldots, 4$, are oriented along the four tetrahedral bonds adjacent to the atom at $\vec{l}$. The sets of

orthonormal functions $\{|b_i\rangle\}$ and $\{|a_i\rangle\}$ can be constructed from the Wannier basis functions by unitary transformations:

$$|b_i(\vec{l})\rangle = \sum_{n=1}^{4} c_{ni}|W_n(\vec{l})\rangle \tag{6a}$$

and

$$|a_i(\vec{l})\rangle = \sum_{n=5}^{8} d_{ni}|W_n(\vec{l})\rangle\,, \tag{6b}$$

where $n = 1$ to 4 are the valence bands, and $n = 5$ to 8 are the conduction bands.

As pointed out by Kane and Kane,[17] a direct computation of the Wannier basis from Eq. (3) would be difficult because of the uncontrolled randomly varying phase factors of $|\psi_{n\vec{k}}\rangle$ as a function of $\vec{k}$. However, there are certain physical quantities that can be computed without actually calculating the Wannier basis functions. For example, the bonding and the antibonding energies are given by the expressions

$$\epsilon_b = \langle b_i(\vec{l})|\hat{H}|b_i(\vec{l})\rangle = \frac{1}{4N}\sum_{n=1}^{4}\sum_{\vec{k}}\epsilon_n(\vec{k}) = \tfrac{1}{4}\int \epsilon\rho_v(\epsilon)\,d\epsilon \tag{7a}$$

and

$$\epsilon_a = \langle a_i(\vec{l})|\hat{H}|a_i(\vec{l})\rangle = \frac{1}{4N}\sum_{n=5}^{8}\sum_{\vec{k}}\epsilon_n(\vec{k}) = \tfrac{1}{4}\int \epsilon\rho_c(\epsilon)\,d\epsilon\,, \tag{7b}$$

where ρ_v and ρ_c are the densities of states per unit cell for the valence bands and the first four conduction bands, respectively.

The alloy calculation starts from the scaled virtual crystal approximation (SVCA) introduced in II. SVCA only treats the periodic part of the Hamiltonian, which, in crystal units,[18] is taken to be the concentration-weighted average of the pure-crystal Hamiltonians. If we denote a pseudobinary (or tenary) semiconductor alloy as A_xB_{1-x} (e.g., A stands for GaP and B for GaAs in GaP_xAs_{1-x}), then the Hamiltonian matrix in SVCA is given by

$$\langle H\rangle = xH_A + (1-x)H_B\,, \tag{8}$$

where H_A and H_B are taken from Eq. (1) and expressed in cu for A and B, respectively. Following the procedure leading from Eq. (3) to Eq. (6), we can define the bonding basis set $\{|b_i(\vec{l})\rangle\}$ and the antibonding basis set $\{|a_i(\vec{l})\rangle\}$ associated with $\langle H\rangle$.

Since the alloy Hamiltonian is not periodic, neither are the Hamiltonian matrix elements expressed in the basis set $\{|b_i(\vec{l})\rangle\}$ and the antibonding basis set $\{|a_i(\vec{l})\rangle\}$. The simplest alloy model assumes that the only important disorder resides in the bond-diagonal matrix elements ϵ_b and ϵ_a. This assumption is justified in the studies reported in I and II. In I, using the BOM, the bond energy differences among compounds were found to be considerably larger than the interbond interactions. In II, a systematic study of the Hamiltonian matrix elements in the local basis showed that the interatomic interactions in the III–V compounds scale[19] as $1/a^2$ (i.e., are nearly constant in cu) while the "atomic" term values exhibited sizable deviations from the $1/a^2$ scaling for the different compounds. Hence, SVCA properly accounts for the long-range alloy interactions, while the local fluctuations in ϵ_a and ϵ_b will be treated with CPA.

To cast this model into mathematical form, lattice vectors $\vec{l}$ in Eq. (6) are assigned to the displacements of the sublattice sites containing the substitutional alloy atoms. For GaP_xAs_{1-x}, for example, $\vec{l}$ will be the lattice vectors for the fcc sublattice on which the P and As atoms are located. Then the Hamiltonian for this simplified alloy model has the form

$$\hat{H}_{\text{alloy}} = \langle\hat{H}\rangle + \sum_{\vec{l}} V_{\vec{l}}\,, \tag{9}$$

where the periodic part $\langle\hat{H}\rangle$ is given in Eq. (8), and the random part has the form

$$V_{\vec{l}} = \sum_{i=1}^{4} |b_i(\vec{l})\rangle\,[\epsilon_b(\vec{l}) - \bar{\epsilon}_b]\langle b_i(\vec{l})| + \sum_{i=1}^{4} |a_i(\vec{l})\rangle\,[\epsilon_a(\vec{l}) - \bar{\epsilon}_a]\langle a_i(\vec{l})|\,. \tag{10}$$

The values of $\epsilon_a(\vec{l})$ and $\epsilon_b(\vec{l})$ depend on which of the substitutional atoms is located at $\vec{l}$, and $\bar{\epsilon}_b$ and $\bar{\epsilon}_a$ are their concentrated weighted average values. We take the values of $\epsilon_a(\vec{l})$ and $\epsilon_b(\vec{l})$ in eV for the atomic pairs that make up the bonds at $\vec{l}$ to be the same as those for the corresponding pure compounds. Thus the present model does not include "off-diagonal" disorder or effects on disorder arising from local strains and charge shifts. We consider these effects to be of higher order than the fluctuations in ϵ_a and ϵ_b treated in the present work.

In CPA theory,[9–11] the configurationally averaged one-electron Green's function is replaced by an effective Green's function G_{eff} adjusted such that on average the atomic scattering matrix vanishes.

Following I, we let $G_{\text{eff}} = (z - \hat{H}_{\text{eff}})^{-1}$, with $\hat{H}_{\text{eff}}$ given by

$$\hat{H}_{\text{eff}}(z) = \langle \hat{H} \rangle + \sum_{\vec{l}} \hat{\sigma}_{\vec{l}} , \tag{11}$$

where the self-energy operator is

$$\hat{\sigma}_{\vec{l}} = \sum_{i=1}^{4} |b_i(\vec{l})\rangle \sigma_b \langle b_i(\vec{l})| + \sum_{i=1}^{4} |a_i(\vec{l})\rangle \sigma_a \langle a_i(\vec{l})| . \tag{12}$$

Then σ_b satisfies a scalar equation

$$\sigma_b(z) = -[\epsilon_b(A) - \bar{\epsilon}_b - \sigma_b] f_b(z) [\epsilon_b(B) - \bar{\epsilon}_b - \sigma_b], \tag{13}$$

where $f_b = \frac{1}{4} F_b$ with $F_b(z)$ [see Eq. (20) in I] shown to be

$$F_b(z) = \int d\epsilon \, \bar{\rho}_v(\epsilon)/(z - \sigma_b - \epsilon), \tag{14}$$

and $\bar{\rho}_v(\epsilon)$ is the valence-band density of states in SVCA. $\sigma_a(z)$ satisfies a similar equation.

Thus, the input to the CPA calculation includes the SVCA densities of states $\bar{\rho}_v$ and $\bar{\rho}_c$, the bonding and antibonding energies ϵ_b and ϵ_a for the pure compounds given by Eqs. (7a) and (7b) and the concentration x. The calculation of these quantities requires numerical integrations over the first Brillouin zone, which are carried out using an efficient technique reported previously.[20] The solution for the CPA self-energies σ_b and σ_a can then be found easily using an iteration method.[21]

Once the self-energies are determined, a variety of quantities can be calculated. The alloy conduction and valence-band density of states are just[11]

$$\rho_c(\epsilon) = -\frac{1}{\pi} \operatorname{Im} F_a(\epsilon + i0) \tag{15a}$$

and

$$\rho_v(\epsilon) = -\frac{1}{\pi} \operatorname{Im} F_b(\epsilon + i0) . \tag{15b}$$

If the self-energies are not too large, the spectral density functions[10]

$$\rho_n(E, \vec{k}) = -\operatorname{Im}\{[E - \bar{\epsilon}_n(\vec{k}) - \sigma(E)]^{-1}\}/\pi$$

will have sharp peaks at E values such that

$$E - \bar{\epsilon}_n(\vec{k}) - \eta(E) = 0 , \tag{16}$$

where $\sigma(E) = \eta(E) - i\gamma(E)$. The energy solution E from Eq. (16) can then be regarded as the band energies in CPA, while the imaginary parts of the self-energy $\gamma(E)$ is the broadening at E due to alloy scattering. Thus, the CPA results contain the ingredients for a detailed study of alloy band structures and transport properties.

III. PARAMETRIZATION OF THE PURE-CRYSTAL BAND STRUCTURES

Since the results of our alloy calculation are sensitively dependent on the input band structures of the constituent compounds, their selection requires special care. In II, a parametrization method was designed to fix the effective masses and symmetry-point energies of states adjacent to the band gaps precisely to well established values. Numerical results for the parametrized bands of GaAs, GaP, InP, and AlAs were reported in II. However, since that time some parameters have been slightly refined to improve the agreement with experiment. The modified selection procedure and the new parameter set are described next.

The procedure begins with the calculation of the overlap matrix $S(\vec{k})$ and the Hamiltonian matrix $H_0(\vec{k})$ of Eq. (1) using the universal Gaussian basis set and empirical pseudopotentials.[22] Then the experimental photoelectric thresholds[23] are used to fix the Γ_{15v} level with respect to the vacuum level. Finally, the nine adjustable interactions in $H_1(\vec{k})$ of Eq. (1) are determined by fitting the Γ_{15v}, Γ_{1c}, Γ_{15c}, X_{5v}, X_{1c}, X_{3c}, L_{3v}, and L_{1c} band energies, and the effective mass m_c^* at Γ_{1c}. These input band energies and m_c^* are selected from a combination of experimental data: the calculated bands for GaP, GaAs, and InP by Chelikowsky and Cohen (CC)[24]; and calculated bands for AlAs by Caruthers and Lin-Chung (CL).[25] The experimental data are used only to improve the accuracy of m_c^* and the low-lying conduction-band energies Γ_{1c}, X_{1c}, X_{3c}, and L_{1c}. Table I lists the values adopted for these band quantities and the parameters for $H_1(\vec{k})$.

For GaAs, the parameters listed in Table I are identical to those in II. The Γ_{1c}, X_{1c}, and X_{3c} energies of GaAs in Table I are different from the CC values but are those used successfully by Aspens.[26] For GaP, the 2.88 eV listed for the Γ_{1c} level is the same as that in CC and also agrees with experiment.[27,28] The values 2.34 eV and 2.64 eV for the X_{1c} and X_{3c} levels, respectively, in Table I are slightly different from the values 2.16 eV and 2.71 eV in CC but are in better agreement with low-temperature optical data.[28] The experimental situation for L_{1c} in GaP is less certain. Aspens estimated a value of 2.73 eV at 77 K.[26] This corresponds to 2.74 eV at 0 K, which is 0.05 eV lower than the value given by CC. For InP, the Γ_{1c} level is taken to be 1.42 eV based on the experimental result of Turner *et al.*[29] With an estimated 0.9 ± 0.02 eV for the $X_{1c}-\Gamma_{1c}$ separation by Dumbe *et al.*[30] added, the X_{1c} level is at 2.32 eV. The 2.07-eV and 2.84-eV values

TABLE I. The lower conduction-band energies (in eV) and effective masses at Γ_{1c} (in units of the free-electron mass) used as input parameters of the band structures for AlAs, GaAs, GaP, and InP; and the parameters (in Cu) obtained for $H_1(\vec{k})$. Also listed are the lattice constants a (in units of the Bohr radius) and the calculated bonding energies ϵ_b and antibonding energies ϵ_a (in eV).

	AlAs	GaAs	GaP	InP
Γ_{1c}	2.90	1.52	2.88	1.42
X_{1c}	2.24	1.98	2.34	2.32
X_{3c}	2.89	2.38	2.64	2.84
L_{1c}	2.48	1.82	2.74	2.07
m_c^*	0.15	0.067	0.17	0.077
δE_s^A	−0.1210	−0.0803	0.0201	−0.0966
δE_s^C	0.0583	0.0122	0.0348	0.0579
δE_p^A	−0.0658	−0.0385	−0.0219	−0.0424
δE_p^C	0.0161	0.0157	0.0110	0.0161
δh_{ss}	−0.0465	−0.0461	0.0256	−0.0310
δh_{sx}	0.0442	0.0579	−0.0168	0.0581
δh_{xs}	0.0344	−0.0122	0.0320	0.0263
δh_{xx}	−0.0453	−0.0416	−0.0343	−0.0429
δh_{xy}	0.0287	−0.0007	0.0060	0.0200
a	10.643	10.687	10.299	11.095
ϵ_b	−10.70	−10.76	−10.97	−10.44
ϵ_a	1.32	0.81	1.40	1.55

assigned, respectively, to the L_{1c} and X_{3c} levels of InP make the separations $X_{1c} - L_{1c}$ and $X_{3c} - X_{1c}$ roughly the same as those in CC. For AlAs, the only level clearly established by experiment is the minimum gap $X_{1c} = 2.238$ eV by Lorenz et al.[31]

The quoted experimental values[32–34] for Γ_{1c} at room temperature range from 2.90 to 3.23 eV, which are at least 0.1 eV higher than the calculated value by CL. The experimental uncertainty seems to arise from the difficulty in preparing high-quality AlAs crystals, and because the Γ_{15v} to Γ_{1c} direct-transition edge in the optical spectra tends to be obscured by excitons and indirect transitions. On the other hand, the direct gaps in $Al_xGa_{1-x}As$ alloys for $x < 0.45$ have been well resolved experimentally by Dingle *et al.*[35] We found that a value of 3.0 eV or higher for the Γ_{1c} level of AlAs leads to poor agreement with this set of clear experimental data. The lower-bound value 2.90 eV is a more reasonable choice. The L_{1c} and X_{3c} levels in AlAs are even more uncertain experimentally; we adopted the values of 2.48 and 2.89 eV calculated by CL. The effective masses m_c^* of the direct-gap compounds GaAs and InP in Table I are the experimentally well established values,[36] while for GaP and AlAs the values adopted are theoretical numbers.[37]

TABLE II. The parametrized band energies (in eV) at Γ, X, and L with respect to the vacuum level and the effective masses at Γ (in units of the free-electron mass) for the four constituent compounds.

	AlAs	GaAs	GaP	InP
Γ_{15v}	−5.76	−5.50	−5.70	−5.70
Γ_{1c}	−2.86	−3.98	−2.82	−4.28
X_{5v}	−8.08	−8.39	−8.40	−7.76
X_{1c}	−3.52	−3.52	−3.36	−3.38
X_{3c}	−2.87	−3.12	−3.06	−2.86
L_{3v}	−6.73	−6.38	−6.61	−6.48
L_{1c}	−3.28	−3.68	−2.96	−3.63
$m_c^*(\Gamma_{1c})$	0.154	0.067	0.169	0.078
$m_l[100]$	−0.146	−0.068	−0.113	−0.081
$m_h[100]$	−0.440	−0.449	−0.460	−0.494
$m_l[111]$	−0.108	−0.060	−0.114	−0.071
$m_h[111]$	−1.062	−1.132	−1.177	−1.188

To illustrate the features of the parametrized bands, the band structures for AlAs, GaP, GaAs, and InP along symmetry directions are plotted in Figs. 1(a)–1(d). Finally, some band energies at Γ, X, and L, and the effective masses at Γ_{1c} associated with these parametrized band structures are listed in Table II.

IV. CALCULATED ALLOY BAND STRUCTURES

Starting from band structures for the constituent compounds obtained in Sec. III and using the interpolation procedure presented in Sec. II, the CPA calculations have been done for $Al_xGa_{1-x}As$, GaP_xAs_{1-x}, and $Ga_xIn_{1-x}P$. Before presenting the specific results for each system, it is useful to discuss certain general aspects of the calculation.

There are two mechanisms in the present model that can produce a nonlinear concentration dependence of the band energies. The first is the scaling of the constituent Hamiltonian matrices inherent in the SVCA. Generally, this nonlinear effect becomes progressively more important the larger the differences between the constituent compounds' lattice constants and energies. However, detailed variations are governed by the structure of the Hamiltonian matrices of the constituent compounds for the specific $\vec{k}$ involved.

The second mechanism causing a nonlinear concentration dependence of the band energies arises

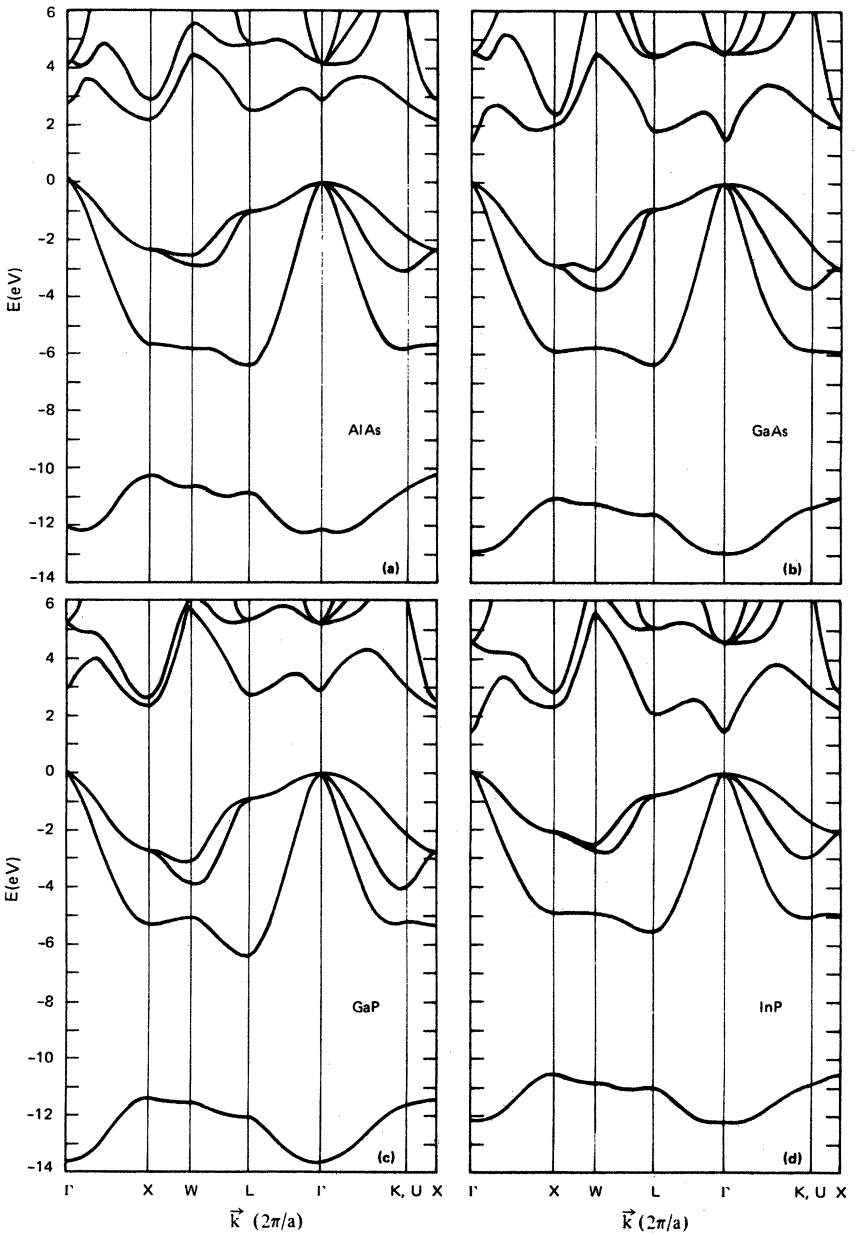

FIG. 1. The parametrized band structures of the compounds (a) AlAs, (b) GaAs, (c) GaP, and (d) InP. The zero of energy in each case is the top of the valence band Γ_{15v}.

from the alloy disorder. In the present model, the alloy scattering is governed by the fluctuations in ϵ_b and ϵ_a measured by the differences $\delta_b \equiv \epsilon_b(A) - \epsilon_b(B)$ and $\delta_a \equiv \epsilon_a(A) - \epsilon_a(B)$. The quantities δ_a and δ_b are referred to as scattering strengths in CPA theory. The values in Table I indicate that the important disorder in $Ga_xAl_{1-x}As$ and GaP_xAs_{1-x} occurs in the conduction bands where $|\delta_a| = 0.51$ and 0.59 eV while $|\delta_b| = 0.06$ and 0.21 eV, respectively. However, in $Ga_xIn_{1-x}P$, the disorder in the valence bands, where $|\delta_a| = 0.53$ eV, is larger than that in the conduction bands.

Thus, the alloy scattering strengths in the present model are the differences between the centers of gravity of the conduction- (antibonding) band energies and the valence- (bonding) band energies. These results differ from previously proposed alloy scattering strengths: band-gap differences, differences between band edges for each band, and electronegativity differences.[38]

Since the scattering strengths for all three alloys are moderate, a lower-order approximation[10]

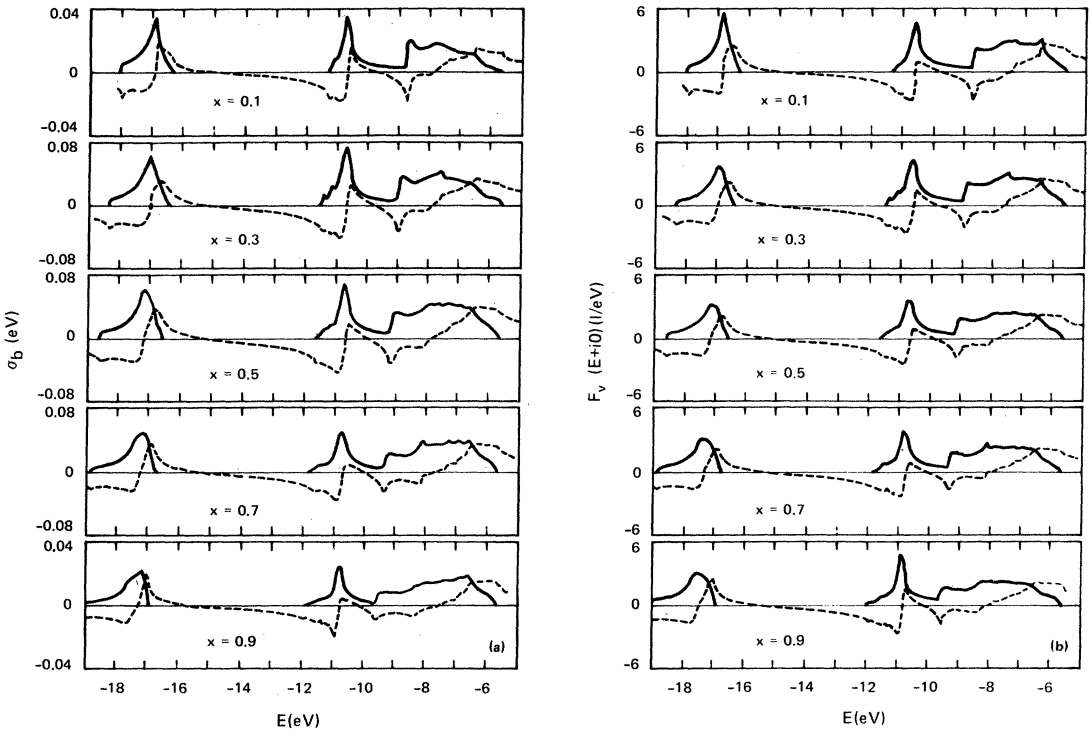

FIG. 2. The real (dashed curves) and imaginary (solid curves) parts of the valence band (a) self-energies and (b) Green's functions as a function of energy relative to the vacuum level for five different concentrations x of the $Ga_xIn_{1-x}P$ alloy.

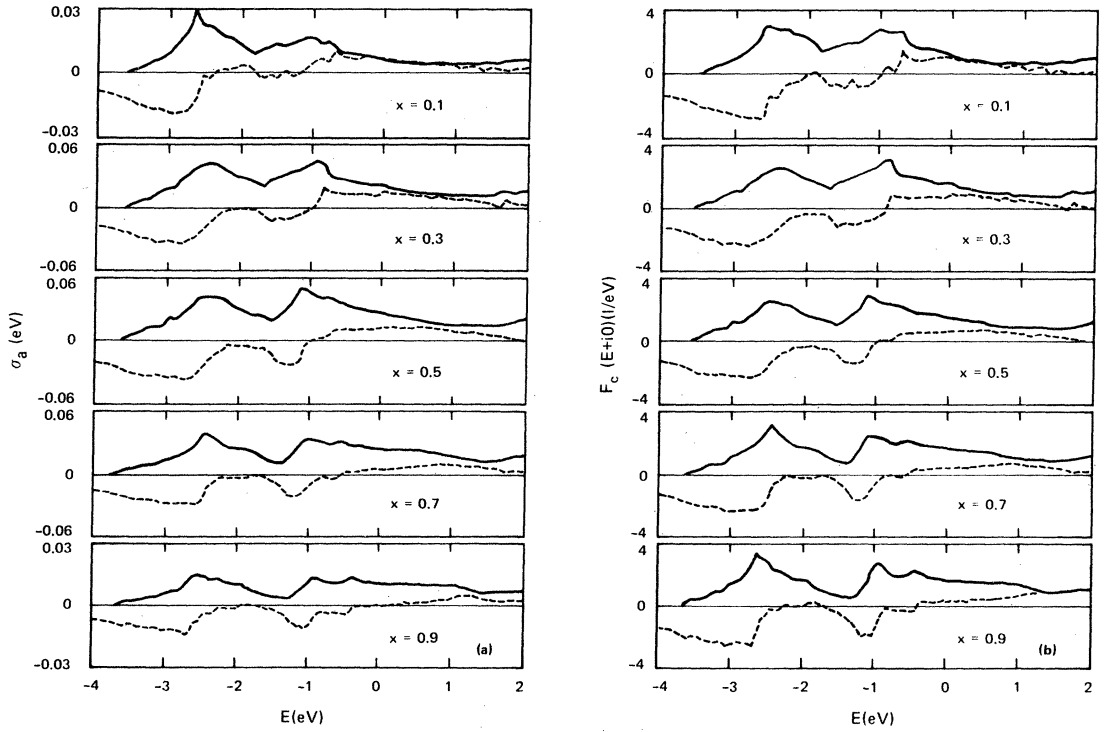

FIG. 3. The real (dashed curves) and imaginary (solid curves) parts of the conduction band (a) self-energies and (b) Green's functions as a function of energy relative to the vacuum level for five different concentrations x of the $Ga_xAl_{1-x}As$ alloy.

to the CPA self-energies in Eqs. (13) and (14),

$$\delta = \tfrac{1}{4}x(1-x)\sigma^2 F, \tag{17}$$

should yield qualitative trends. However, the full self-consistent solution to the CPA equation is needed for quantitative results. Using the iteration technique[21] a convergence for σ to within 0.0001 eV is achieved in no more than 5 iterations at all energies and concentrations for every alloy considered here. The most time-consuming numerical computations are the SVCA densities of states (DOS) $\bar{\rho}_v(E)$ and $\bar{\rho}_c(E)$ needed in Eq. (14). This has to be done accurately for every concentration and on fine energy grids over the entire energy range of the SVCA bands. Representative prospectives of the calculated spectra can be gained by examining plots of the CPA-generated functions σ_b and F_v for the $Ga_xIn_{1-x}P$ alloy displayed in Figs. 2(a) and 2(b), and similar results for σ_a and F_c for the $Ga_xAl_{1-x}As$ alloy depicted in Figs. 3(a) and 3(b). These figures show that Eq. (17) predicts qualitative trends correctly but it does not yield quantitatively accurate self-energies. This means that the usual perturbation calculations cannot accurately account for lifetimes and bowing parameters. However, the scattering strengths δ_a and δ_b for these alloys are still small compared to their respective bandwidths, so alloy disorder has very little effect on the DOS. To demonstrate this point, the DOS derived from CPA (solid curves) and SVCA (dashed curves) for the 50-50 $GaP_{0.5}As_{0.5}$ alloy are plotted in Fig. 4. The SVCA and CPA DOS are essentially the same for the valence bands. The difference in ρ_c between SVCA and CPA is discernible in the plot but it is still too small to be detected by present DOS spectroscopy methods, e.g., the photoelectric spectra. This result is consistent with our conclusion in I and with previous work on SiGe alloys.[39] However, the same conclusion may not be drawn for II–VI compound alloys where the alloy disorder is much larger.[40]

A. $Ga_xAl_{1-x}As$

Figure 5 illustrates the variation of seven symmetry-point energies as a function of the Ga concentration x. All these curves show some nonlinear concentration dependence. Since the experimental band gaps are usually fit to a function of the form[1-4]

$$E = \bar{E} - bx(1-x), \tag{18}$$

where $\bar{E}$ is the average energy $\bar{E} = E_A + (1-x)E_B$, and b is the bowing parameter, we will use Eq. (18) to define b for each state and let b vary with x. Table III lists the values found for b from SVCA and CPA for these seven states and for five Ga concentrations from $x = 0.1$ to 0.9. The actual band energies are obtained at these concentrations from Eq. (16), and b is obtained from Eq. (18) using the end-point values in Table III to find $\bar{E}$ in each case.

First, we see that there is no disorder contribution to the bowing, i.e., no difference between the CPA and SVCA b values, for the valence-band energies. This is because there is essentially no difference in the bonding energies ϵ_b between GaAs and AlAs. However, SVCA alone

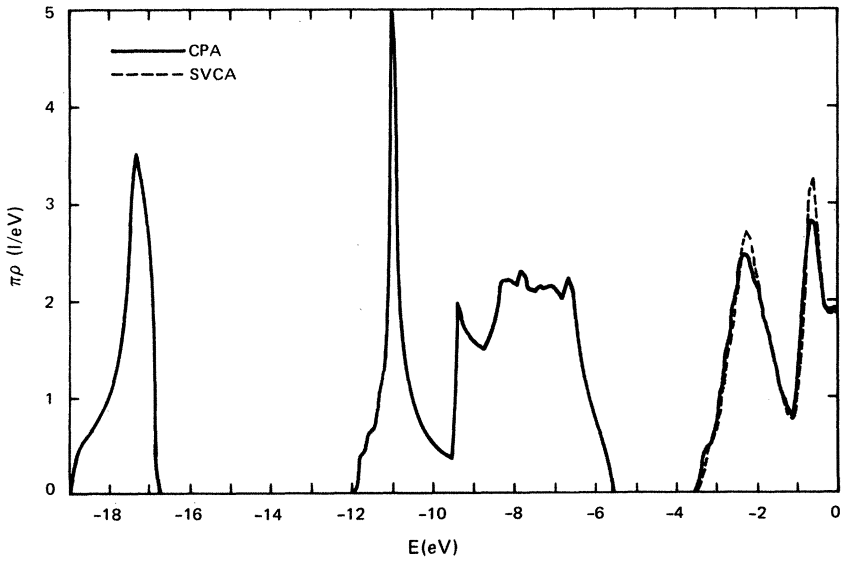

FIG. 4. The CPA (solid curve) and SVCA (dashed curve) predicted density of states as a function of energy relative to the vacuum level for the alloy $GaP_{0.5}As_{0.5}$.

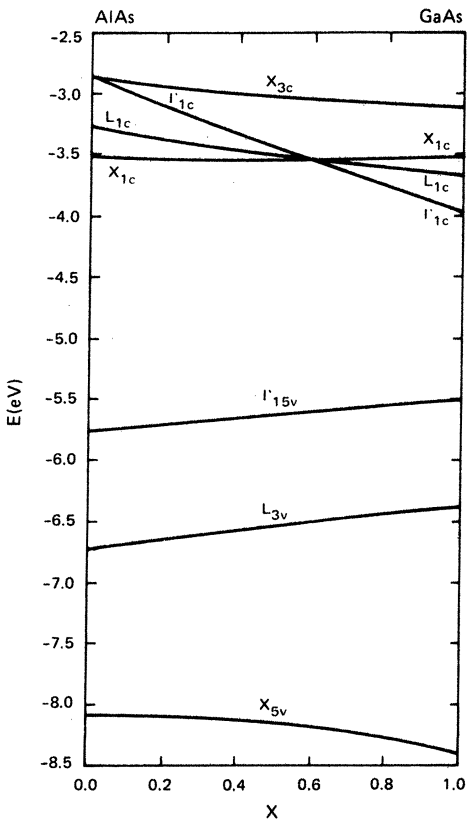

FIG. 5. The indicated symmetry-point energies relative to the vacuum level as functions of concentration x for the alloy $Ga_xAl_{1-x}As$.

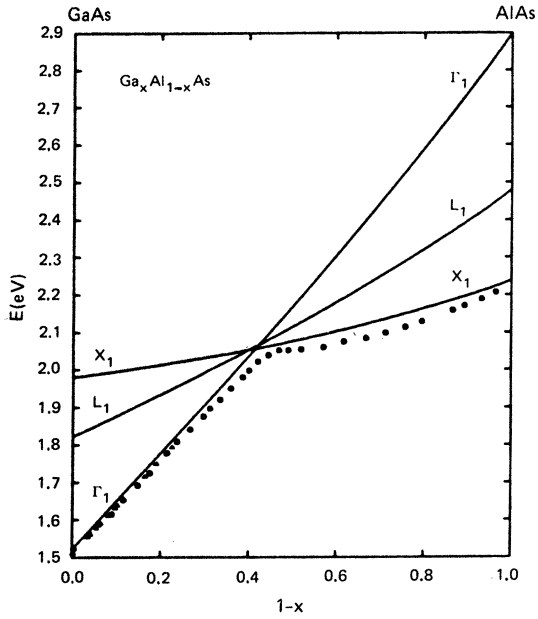

FIG. 6. The theoretical band gaps between the Γ_{1c}, X_{1c}, and L_{1c} states and Γ_{15v} (solid curves labeled Γ_1, X_1, and L_1, respectively) as functions of the Al concentrations $1-x$ for the alloy $Ga_xAl_{1-x}As$. The circles (Ref. 35) and triangles (Ref. 42) are experimental exciton peak positions.

contributes a value $b=-0.07$ eV for the L_{3v} point and -0.35 eV for X_{5v}. By contrast, SVCA contributes little to the bowing of the conduction-band states, whereas the disorder produces a

TABLE III. Bowing parameters b (in eV) defined in Eq. (18) calculated in SVCA and CPA for the seven states at Γ, X, and L for five concentrations x of the $Ga_xAl_{1-x}As$ alloy. Also listed are the effective masses at Γ (in units of free-electron mass) calculated using CPA.

x	0.1		0.3		0.5		0.7		0.9		Average	
	SVCA	CPA	SVCA	CPA	SVCA	CPA	SVCA	CPA	SVCA	CPA	SVCA	CPA
Γ_{15v}	−0.01	−0.02	−0.01	−0.01	−0.01	−0.01	−0.01	−0.01	−0.01	−0.01	−0.01	−0.01
Γ_{1c}	0.02	0.24	0.03	0.18	0.03	0.16	0.03	0.13	0.02	0.11	0.03	0.16
X_{5v}	−0.28	−0.28	−0.31	−0.31	−0.34	−0.34	−0.38	−0.38	−0.43	−0.43	−0.35	−0.35
X_{1c}	0.00	0.15	0.00	0.12	0.00	0.12	0.00	0.11	0.00	0.11	0.00	0.12
X_{3c}	0.01	0.22	0.01	0.17	0.01	0.14	0.01	0.14	0.01	0.13	0.01	0.16
L_{3v}	−0.06	−0.07	−0.06	−0.07	−0.07	−0.07	−0.07	−0.07	−0.07	−0.07	−0.07	−0.07
L_{1c}	0.01	0.19	0.01	0.15	0.01	0.13	0.01	0.12	0.0	0.11	0.01	0.14
m^*	0.148		0.126		0.106		0.093		0.075			
m_l[100]	−0.137		−0.121		−0.104		−0.089		−0.075			
m_h[100]	−0.435		−0.444		−0.444		−0.455		−0.449			
m_l[111]	−0.103		−0.094		−0.084		−0.075		−0.065			
m_h[111]	−0.053		−1.101		−1.111		−1.143		−1.154			

sizable contribution. We also see that the bowing functions b are not constant but vary significantly with x. The bowing of the conduction-band states decreases by roughly a factor of 2 from the Al-rich to the Ga-rich alloys, while for the valence-band state X_{5v}, $|b|$ increases as the Ga concentration increases.

Although it is difficult to identify the physical origin of the asymmetric contributions to b at X_{5v} that arise in SVCA, a qualitative understanding of the skewed x dependence of the conduction-band states' b values arising from disorder can be gleaned from Eq. (17), Figs. 3(a) and 3(b). Notice that the conduction-band states being considered lie close to the bottom of the conduction bands where the magnitude of the $\mathrm{Re}\{F_c\}$ over the range from -3 to -4 eV decreases by about a factor of 2. From Eq. (17), this introduces an energy dependence into the CPA energy shifts η with respect to the SVCA levels.

There is another and perhaps more important mechanism contributing to the x dependence of b arising from higher-order scattering effects to the self-energy that is not included in Eq. (17). Consider the case with $x=0.1$. Since the alloy medium is close to pure AlAs, GaAs cells act as impurity scattering centers. Because ϵ_a in GaAs is 0.51 eV below that in AlAs, the "impurity" scattering for $x=0.1$ will more strongly affect the lower-energy part of the conduction band than the higher-energy part. On the other hand, in the $x=0.9$ case the Al cell serves as the dominant impurity scatterer in the GaAs host lattice. Thus, the lower-energy part of the conduction band will not be affected as much. This explanation is supported by the numerical results displayed in Fig. 3(a), in which the magnitude of η at the bottom of the band for $x=0.1$ is considerably larger than that for $x=0.9$. A similar effect can also be seen from a comparison of the $x=0.3$ and $x=0.7$ cases. This general effect is well illustrated by the numerical results obtained using a simple semiellipse-model density of states.[41]

To compare with experiment, the gaps $\Gamma_1=\Gamma_{1c}-\Gamma_{15v}$, $X_1=X_{1c}-\Gamma_{15v}$, $X_3=X_{3c}-\Gamma_{15v}$, and $L_1=L_{1c}-\Gamma_{15v}$ are plotted in Fig. 6 against the Al concentration $1-x$. Also plotted are the peak positions for excitons determined from photoluminescence (PL) spectra at 2 K by Dingle *et al.*[35] (circles) and by Stingfellow and Kunzel[42] (triangles). After the exciton binding energies are added to these experimental numbers, they should agree well with the theoretical minimum band gaps. In Table III, the Γ_1 gap has a bowing parameter of 0.12 eV at $x=0.1$ and 0.25 eV at $x=0.9$, with an average b value of 0.17 eV. Earlier experiments, most of them done at room temperature, resulted in b values[43] ranging from 0.18 to 0.47 eV.

More recent experiments[44] and analyses[45,46] suggest that the Γ_1 gap varies linearly with x in the direct-gap, Ga-rich concentration range and it has a large bowing parameter beyond the crossover at $1-x_c=0.45$ in the indirect-gap region. All previous theories, mostly because the lattice constants of GaAs and AlAs are nearly the same, predict very small b values for the Γ_1 gap, i.e., -0.04 eV,[7] 0.03 eV,[1] and 0.05 eV.[47] These theoretical results, combined with the uncertainties involved in extracting the Γ_1 gaps from optical data in the indirect-gap region, may be the origin of the suggestion that the bowing of the Γ_1 gap changes abruptly at x_c. Although it is evident from the CPA model why the bowing should be larger on the Al-rich side than on the Ga-rich side, we know of no mechanism that could produce the large abrupt change at x_c referred to above. The calculated X_1-gap curve is seen to be in excellent agreement with the data. The asymmetry in b for X_1 is not as large as that for Γ_1. Our average b for X_1 is 0.14 eV, which is in excellent agreement with the 0.143 eV (Ref. 46) and 0.15 eV (Ref. 47) used in recent analysis, but smaller than the value of Lee *et al.*[48] of 0.245 eV.

Our predicted Γ_1 and X_1 band gaps cross at the critical Al concentration $1-x_c=0.42$, with a minimum gap $E_c=2.06$ eV at this concentration. As the temperatures increase, $1-x_c$ should move to higher Al concentrations and E_c to lower energies. Therefore, our x_c and E_c are consistent with the $1-x_c=0.44$ and $E_c=2.04$ eV obtained by Dingle *et al.*[35] at 2 K, and the room-temperature values of $1-x_c=0.45$, $E_c=1.985$ eV and $1-x_c=0.45$, $E_c=1.97$ eV used in recent analysis.[46,47] However, our values are slightly higher than the $1-x_c=0.405$ and $E_c=1.953$ eV used by Lee *et al.*,[48] but distinctly larger than the previous experimental value[49] $1-x_c=0.37$ and the previous calculated value[7] of $1-x_c=0.3$. Recently Temkin and Keramidas[46] showed that a value of $1-x_c\doteq 0.37$ led to inconsistent results with experiments on the concentration dependence of the conductivity. The L_1 gap is comparatively less well determined experimentally.[45,46]

The spectral widths $\gamma(E)$ for E at the CPA band energies provide a measure of the alloy scattering lifetime. Figures 2 and 3 show that γ is a sensitive function of energy and concentration. These strong x dependences of γ will inevitably be reflected in transport and optical properties, particularly at the crossover concentration. However, it is worth emphasizing once more[50] that at the band edges, γ becomes very small, so there will be little alloy broadening of the modulation spectra E_0 lines in the direct-gap alloys

even though the bowing is significant.

Another quantity closely related to the transport properties is the effective mass. Table III lists the effective mass m^* at Γ_{1c} and the heavy m_h and light m_l hole masses along both the [100] and [111] directions for the Γ_{15v} states. The CPA results are bowed only slightly down from the average values. The variations arising in SVCA are the major determining factors on effective masses. In I, we show that the alloy disorder influences the effective mass through the energy derivative of the real part of the self-energy η, $m_{\mathrm{CPA}} = m_{\mathrm{SVCA}}(1 - d\eta/dE)$. The disorder contribution can be estimated by examination of Figs. 2 and 3, and at most changes the SVCA value by about 2%. Therefore, the usual linear interpolation for m^* used in transport analysis is nearly correct for this system.

B. GaP_xAs_{1-x}

Figure 7 contains plots of seven band energies as a function of P concentration, and Table IV lists the corresponding bowing functions b for five alloy concentrations. Since the scattering

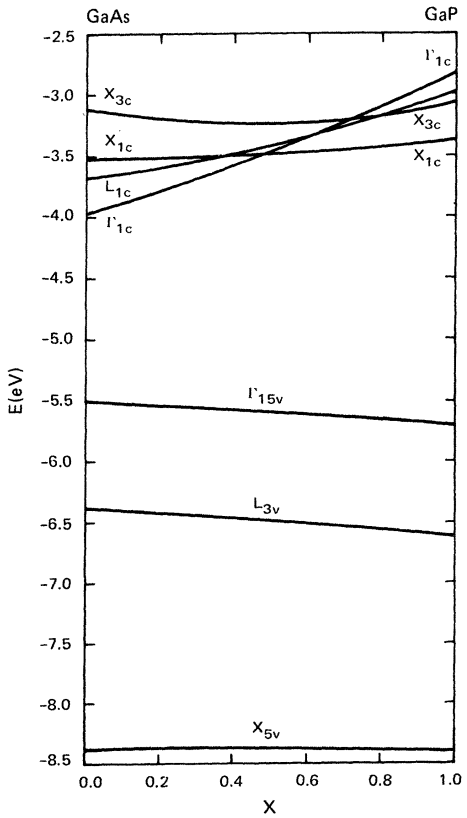

FIG. 7. The indicated symmetry-point energies relative to the vacuum level as functions of concentration x for the alloy GaP_xAs_{1-x}.

parameters for GaP_xAs_{1-x} are similar to those in $Ga_xAl_{1-x}As$, namely $|\delta_a| > |\delta_b|$ with GaAs having the lower ϵ_a, the asymmetric contributions to b due to alloy disorder follow a similar pattern. However, the bowing for the conduction-band energies resulting from SVCA are considerably larger in GaP_xAs_{1-x} than in $Ga_xAl_{1-x}As$.

In Fig. 8 the three low-lying conduction-band gaps Γ_1, X_1, and L_1 are plotted as a function of concentration. The exciton peak positions in the PL spectra measured at 6 K by Onton and Foster[51] (crosses) and at 77 K by Nelsen *et al.*[52] (circles) and the peak positions in the cathodoluminescence (cl) spectra at 30 K by Marciniak and Wittry[53] (triangles) are also plotted for comparison. Once the exciton binding energies are added, our X_1 curve will be in excellent agreement with the data of Onton and Foster.

The Γ_1 and X_1 curves are also consistent with the cl spectra. However, a few meV rigid shift is needed to bring the Γ_1 curve into register with the measurements by Nelsen *et al.* From Table IV, the average b value for the Γ_1 gap over all x is 0.26 eV, while the average value in the direct-gap region only is 0.23 eV. Thus, our calculated bowing parameter for Γ_1 is slightly larger than the range of values from 0.17 to 0.21 eV quoted from previous analyses.[26,54] The dielectric model[1] predicted 0.30 eV with contributions of 0.21 eV from the "intrinsic" term and 0.09 eV from disorder. For comparison, we find average contributions of 0.11 eV from SVCA and 0.15 eV from disorder. For the X_1 gap, our calculated average b value is 0.22 eV, which lies between the 0.143 (Ref. 54) to 0.16 (Ref. 26) eV used in prior analysis and the 0.267 eV deduced by Onton and Foster.[51] With X_1 and Γ_1 as described, we find the indirect- to direct-gap crossover P concentration is at $x_c = 0.48$ with $E_c = 2.10$ eV. Our x_c lies between the values $x_c = 0.45$ at 77 K measured by Nelsen *et al.*[52] and the $x_c = 0.51$ at 30 K measured by Marciniak and Wittry.[53] The L_1 gap has a much larger bowing parameter $b = 0.45$ eV than the other two gaps. This value is also larger than previously quoted values which range from 0.16 (Ref. 26) to 0.25 eV.[2] However, the experimental situation for the L_1 gap in alloys is still very uncertain. The behavior of m^* in Table IV is similar to that for $Ga_xAl_{1-x}As$.

C. $Ga_xIn_{1-x}P$

As mentioned previously, in this alloy the disorder in the valence band is larger than in the conduction band ($\delta_b = 0.53$ eV $> \delta_a = 0.15$ eV), which is opposite to the arrangement in the other two alloy systems. Thus the nonlinear depen-

TABLE IV. Bowing parameters b (in eV) defined in Eq. (18) calculated in SVCA and CPA for the seven states at Γ, X, and L for five concentrations x of the GaP_xAs_{1-x} alloy. Also listed are the effective masses at Γ (in units of free-electron mass) calculated using CPA.

x	0.1		0.3		0.5		0.7		0.9		Average	
	SVCA	CPA	SVCA	CPA	SVCA	CPA	SVCA	CPA	SVCA	CPA	SVCA	CPA
Γ_{15v}	−0.01	−0.03	−0.01	−0.03	−0.01	−0.03	−0.01	−0.03	−0.01	−0.03	−0.01	−0.03
Γ_{1c}	0.09	0.20	0.09	−0.22	0.10	0.25	0.10	0.28	0.12	0.23	0.10	0.23
X_{5v}	−0.11	−0.11	−0.11	−0.10	−0.11	−0.10	−0.10	−0.10	−0.11	−0.10	−0.11	−0.10
X_{1c}	0.02	0.17	0.02	0.17	0.02	0.17	0.03	0.19	0.03	0.22	0.03	0.19
X_{3c}	0.37	0.53	0.39	0.55	0.40	0.57	0.41	0.59	0.39	0.67	0.39	0.58
L_{3v}	−0.01	−0.03	−0.01	−0.03	−0.01	−0.03	−0.01	−0.03	−0.01	−0.04	−0.01	−0.03
L_{1c}	0.24	0.37	0.24	0.38	0.24	0.40	0.25	0.42	0.26	0.52	0.24	0.42
m^*	0.077		0.095		0.115		0.135		0.159			
m_l[100]	−0.076		−0.092		−0.110		−0.129		−0.148			
m_h[100]	−0.460		−0.455		−0.465		−0.465		−0.465			
m_l[111]	−0.065		−0.076		−0.088		−0.099		−0.109			
m_h[111]	−1.154		−1.165		−1.177		−1.188		−1.188			

dences caused by disorder become more important in the valence than in the conduction bands. However, as Table V shows, the SVCA contributions to the bowing of the conduction bands are considerably larger than those of the valence bands.

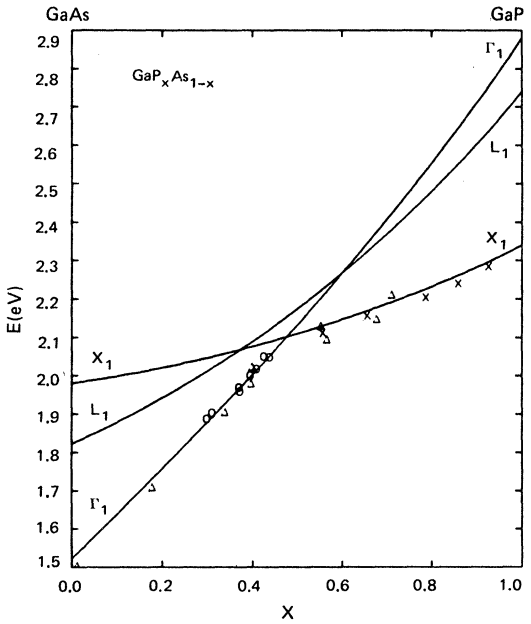

FIG. 8. The theoretical band gaps between the Γ_{1c}, X_{1c}, and L_{1c} states and Γ_{15v} (solid curves labeled Γ_1, X_1, and L_1, respectively) as functions of the P concentration x for the alloy GaP_xAs_{1-x}. The circles (Ref. 52), triangles (Ref. 53), and crosses (Ref. 51) are experimental exciton peak positions.

In Fig. 9 the usual seven band energies as a function of Ga concentration x are plotted. Again, for comparison with experiment, the three gaps Γ_1, X_1, and L_1 are plotted as a function of x in Fig. 10. The experimental data presented in Fig. 10 are the exciton peak positions in the PL spectra taken at 2 K by Onton and Chicotka[55] (crosses), at 4.2 K by Joullie and Alibert[56] (circles), and at 77 K by Macksey *et al.*[57] (triangles). Although the data are more scattered than those in Figs. 6 and 8, our calculated minimum gaps correlate reasonably well with this somewhat scattered data set. Our calculated average b values for the Γ_1, X_1, and L_1 gaps are 0.40, 0.17, and 0.41 eV, respectively. The value of $b=0.40$ eV for the Γ_1 gap coincides with the lower end of the experimental range from 0.40 to 0.88 eV.[2,58,59] The value of b for the X_1 gap is considerably smaller than those for Γ_1 or L_1 but is in excellent agreement with the 0.16 eV quoted by Onton.[60] The experimental b value for the L_1 gap is less certain, but our calculated value of 0.41 eV is in accord with the 0.34 eV bowing parameter measured for the E_1 optical gap.[1,2]

The critical Ga concentration x_c for the band crossing is predicted to lie at 0.66 with $E_c=2.29$ eV. Onton and Chicotka[55] used a linear x dependence for the X_1 gap and their highly bowed Γ_1 gap to estimate a value of $x_c=0.74$ and $E_c=2.33$ eV at 2 K. If a value of $b=0.16$ for the X_1 gap is used, x_c will decrease by 0.03. A smaller bowing of their Γ_1 gap will further lower x_c to

TABLE V. Bowing parameters b (in eV) defined in Eq. (18), calculated in SVCA and CPA for the seven states at Γ, X, and L for five concentrations x of the $Ga_xIn_{1-x}P$ alloy. Also listed are the effective masses at Γ (in units of free-electron mass) calculated using CPA.

x	0.1		0.3		0.5		0.7		0.9		Average	
	SVCA	CPA	SVCA	CPA	SVCA	CPA	SVCA	CPA	SVCA	CPA	SVCA	CPA
Γ_{15v}	−0.03	−0.10	−0.03	−0.11	−0.03	−0.11	−0.03	−0.12	−0.03	−0.14	−0.03	−0.11
Γ_{1c}	0.26	0.27	0.27	0.28	0.28	0.28	0.29	0.30	0.31	0.32	0.28	0.29
X_{5v}	−0.07	−0.09	−0.08	−0.06	−0.08	−0.05	−0.08	−0.02	−0.10	−0.03	−0.08	−0.05
X_{1c}	0.05	0.06	0.05	0.06	0.05	0.06	0.06	0.06	0.06	0.07	0.05	0.06
X_{3c}	0.19	0.20	0.20	0.21	0.21	0.22	0.22	0.23	0.20	0.21	0.21	0.22
L_{3v}	0.00	−0.17	0.00	−0.16	0.00	−0.15	0.00	−0.15	0.00	−0.13	0.00	−0.15
L_{1c}	0.28	0.29	0.29	0.30	0.29	0.30	0.30	0.31	0.31	0.32	0.29	0.30
m^*	0.086		0.102		0.120		0.138		0.159			
m_l[100]	−0.089		−0.106		−0.122		−0.141		−0.150			
m_h[100]	−0.506		−0.506		−0.488		−0.494		−0.471			
m_l[111]	−0.077		−0.087		−0.097		−0.107		−0.112			
m_h[111]	−1.224		−1.250		−1.224		−1.250		−1.188			

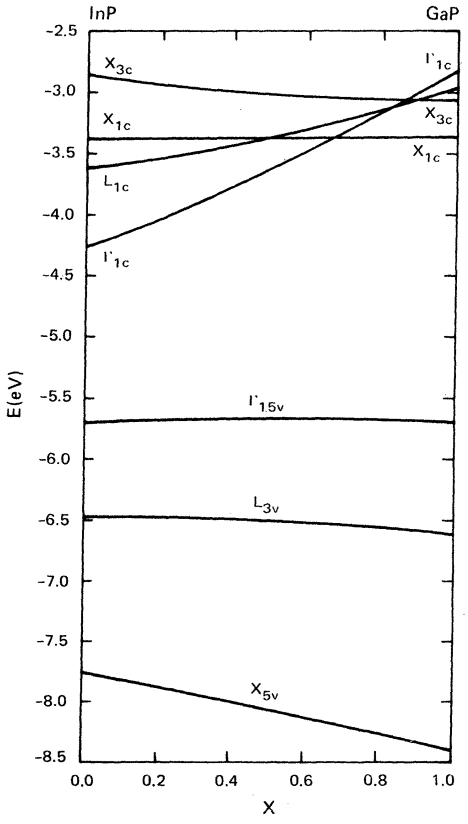

FIG. 9. The indicated symmetry-point energies relative to the vacuum level as a function of concentration x for the alloy $Ga_xIn_{1-x}P$.

below 0.70. Our values are close to the $x_c = 0.69 \pm 0.02$ and $E_c = 2.32 \pm 0.01$ eV for $T < 10$ K found by Joullie and Alibert.[56] Finally, the effective masses listed in Table V again behave in a way

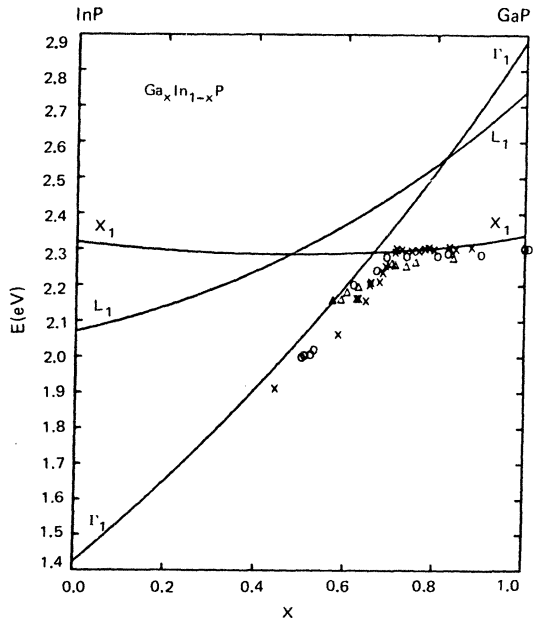

FIG. 10. The theoretical band gaps between the Γ_{1c}, X_{1c}, and L_{1c} states and Γ_{15v} (solid curves labeled Γ_1, X_1, and L_1, respectively) as functions of the Ga concentration x for the alloy $Ga_xIn_{1-x}P$. The circles (Ref. 56), triangles (Ref. 57), and crosses (Ref. 55) are experimental exciton peak positions.

similar to those of $Ga_xAl_{1-x}As$ and GaP_xAs_{1-x}; the CPA m^* is just slightly bowed below the SVCA values.

Thus, the concentration variations of the bands for the three alloy systems considered, where one constitutent is a direct- and the other is an indirect-gap semiconductor, are quite similar. There is in each case a single minimum band-gap crossing, although in GaAlAs the three states almost merge at the crossover concentration. These results are consistent with the analysis of donor levels in GaPAs (Ref. 26) and GaAlAs[35] but differ from the two-crossover model conjectured by Pitt *et al.*[61]

V. SUMMARY AND DISCUSSION

We have presented a CPA method designed to interpolate detailed alloy band structures between those of the pure constituents. Comparison between experiments and our calculated results for $Al_xGa_{1-x}As$, GaP_xAs_{1-x}, and $Ga_xIn_{1-x}P$ demonstrates the accurate quantitative nature of the predictions. The band structures and alloy-scattering information that can be obtained have far broader applications than we have discussed here, e.g., detailed calculations of the optical and transport properties. Furthermore, since the concentration variation of the conduction- and valence-band edges are separately calculated, the energy steps at heterojunctions[62] can be determined.

The present calculation represents perhaps the simplest realistic model. It uses only four simple basis orbitals per atom. The long-range interactions are treated in a scaled virtual crystal approximation, while the alloy disorder appears only in the diagonal matrix elements ϵ_a and ϵ_b. In the absence of reliable information about the effects of potential renormalization on ϵ_a and ϵ_b in alloys, we take the values to be the same as those in the pure compounds. This seems to be justified in view of the accuracy of our results and the recent self-consistent vacancy calculations[63,64] for Si, where it is shown that the impurity potential is quite localized.

One feature not treated in our model is the effect of the "off-diagonal" disorder in the local bonding to antibonding interactions and in the nearest bond-to-bond matrix elements. We have demonstrated in II that the disorder in these terms is significantly smaller than the ones we have treated. Although this formalism can be extended easily to include off-diagonal disorder, its implementation would drastically increase the computational complexity. Until more reliable transition-matrix elements are available to make the small differences meaningful, the inclusion of this disorder may be counterproductive. These matrix elements may be improved by applying Kane's[17] real-space Wannier-basis construction to disordered alloys.

Although the four-orbitals–per-atom basis produces good band energies, it yields poor charge densities.[15] Improvements will result from increasing the number of basis functions. This can be accomplished without spoiling the simple picture of the bonding and antibonding basis by using Louie's phase-dependent chemical orbitals.[65]

However, there is an immediate modification needed to extend the application of this method to alloys with heavier elements. This is the treatment of relativistic effects, particularly the spin-orbit interactions. Techniques for dealing with relativistic effects in the tight-bonding model are already available[66,67] for pure semiconductors and alloys, and they should be easily absorbed into our alloy model. Once this is done, calculations of the properties of all the pseudobinary alloys—the III–V and the II–VI compounds including the important HgCdTe (Ref. 68) system—will be accessible to this method.

ACKNOWLEDGMENT

We gratefully acknowledge support for this work from the U.S. Department of Energy under Contract No. DE-AS 50-79 ER 10379.

[1]J. A. Van Vechten and T. K. Bergstresser, Phys. Rev. B 1, 3351 (1970).
[2]R. Hill, J. Phys. C 7, 521 (1974).
[3]R. Hill, J. Phys. C 7, 516 (1974).
[4]J. A. Van Vechten, O. Berolo, and J. C. Woolley, Phys. Rev. Lett. 29, 1400 (1972).
[5]O. Berolo, J. C. Woolley, and J. A. Van Vechten, Phys. Rev. B 8, 3794 (1973).
[6]R. H. Parmenter, Phys. Rev. 97, 587 (1955).
[7]A. Balderschi, E. Hess, K. Maschke, H. Numann, K-R. Schulze, and K. Unger, J. Phys. C 10, 4709 (1977).
[8]J. W. Harrison and J. R. Hauser, Phys. Rev. B 13, 5347 (1976); J. Appl. Phys. 47, 292 (1976); J. R. Hauser, M. A. Littlejohn, and T. H. Glisson, Appl. Phys. Lett. 28, 458 (1976).
[9]Paul Soven, Phys. Rev. 156, 809 (1967).
[10]B. Velicky, S. Kirkpatrick, and H. Ehrenreich, Phys. Rev. 175, 747 (1968).

[11]A.-B. Chen and A. Sher, Phys. Rev. B 17, 4726 (1978) (referred to as I).
[12]W. A. Harrison, Phys. Rev. B 8, 4487 (1973); W. A. Harrison and S. Circaci, *ibid.* 10, 1516 (1974).
[13]P. T. Pantelides and W. A. Harrison, Phys. Rev. B 11, 3006 (1975).
[14]E. O. Kane, Phys. Rev. B 13, 3478 (1976).
[15]D. J. Chadi, Phys. Rev. B 16, 3572 (1977).
[16]A.-B. Chen and A. Sher, Phys. Rev. B 22, 3886 (1980) (to be referred to as II).
[17]E. O. Kane and A. B. Kane, Phys. Rev. B 17, 2691 (1978).
[18]In crystal units the energy is represented by a dimensionless parameter ϵ. The conversion from ϵ to E in rydbergs is $E=\epsilon(2\pi/a)^2$, where a is the lattice constant in units of the Bohr radius.
[19]W. A. Harrison, in *Festkörperprobleme*, edited by J. Treusch (Frieder, Vieweg, Braunschweig, 1977), Vol. XVII, p. 135.
[20]A.-B. Chen, Phys. Rev. B 16, 3291 (1977).
[21]A.-B. Chen, Phys. Rev. B 7, 2230 (1973).
[22]We used the empirical pseudopotentials for GaAs, GaP, and InP obtained by M. L. Cohen and T. K. Bergstresser, Phys. Rev. 141, 789 (1966). For AlAs, those in Ref. 25 are used.
[23]N. J. Shevichik, J. Tejeda, and M. Cardona, Phys. Rev. B 9, 2627 (1974), Table III. For AlAs, we used the difference of −0.26 eV between GaAs and AlAs found by W. R. Frensley and H. Kroemer, J. Vac. Sci. Technol. 13, 810 (1976).
[24]J. R. Chelikowsky and M. L. Cohen, Phys. Rev. B 14, 556 (1976).
[25]E. Caruthers and P. J. Lin-Chung, Phys. Rev. B 17, 2705 (1978).
[26]D. E. Aspnes, Phys. Rev. B 14, 5331 (1976).
[27]D. D. Sell and P. Lawaetz, Phys. Rev. Lett. 26, 311 (1971).
[28]D. J. Dean, G. Kaminsky, and R. B. Zettersrom, J. Appl. Phys. 38, 3551 (1967).
[29]W. J. Turner, W. E. Resse, and G. D. Pettit, Phys. Rev. 136, 1467 (1964).
[30]W. P. Dambe, M. R. Lorenz, and G. D. Pettit, Phys. Rev. B 1, 4668 (1970).
[31]M. R. Lorenz, R. Chicotka, and G. D. Pettit, Solid State Commun. 8, 693 (1970).
[32]C. A. Mead and W. G. Spitzer, Phys. Rev. Lett. 11, 358 (1963).
[33]W. M. Yim, J. Appl. Phys. 42, 2854 (1971).
[34]B. Monemar, Solid State Commun. 8, 2121 (1970).
[35]R. Dingle, R. A. Logan, and J. R. Arthur, J. Ins. Phys., Conf. Ser. 33A, 210 (1977).
[36]For example, see J. C. Phillips, in *Bonds and Bands in Semiconductors* (Academic, New York, 1973), Table 5.1.
[37]For GaP, the theoretical value is obtained from P. Lawaetz, Phys. Rev. B 4, 3460 (1971); for AlAs, we use the value obtained from the band calculation by D. J. Stükel and R. N. Euwema, Phys. Rev. 188, 1193 (1969).
[38]M. A. Littlejohn, J. R. Hauser, T. H. Glisson, D. K. Ferry, and J. W. Harrison, Solid-State Electron. 21, 107 (1978).
[39]D. A. Stroud and H. Ehrenreich, Phys. Rev. B 2, 3197 (1970).
[40]W. G. Kistler and A.-B. Chen, Bull. Am. Phys. Soc. 24, 466 (1979); W. G. Kistler, Master's thesis, Auburn University, 1979 (unpublished).
[41]The effects on the energy dependence of the self-energy caused by the sign of the disorder parameter and the concentration can best be understood qualitatively by examining Fig. 5 in Ref. 10.
[42]G. B. Stringfellow and H. Künzel, J. Appl. Phys. 51, 3254 (1980).
[43]H. C. Casey, Jr. and M. B. Panish, J. Appl. Phys. 40, 4910 (1969) gave a value of 0.18 eV while A. Onton, M. R. Lorenz, and J. M. Woodall, Bull. Am. Phys. Soc. 16, 371 (1971) quoted a value of 0.47 eV. For other earlier experimental data see the references in Ref. 7.
[44]B. Monemar, K. K. Shih, and G. D. Pettit, J. Appl. Phys. 47, 2604 (1976).
[45]H. C. Casey, Jr., J. Appl. Phys. 49, 3684 (1978).
[46]H. Temkin and V. G. Keramidas, J. Appl. Phys. 51, 3269 (1980).
[47]D. D. Sell, in *Proceedings of the Eleventh International Conference on Physics of Semiconductors, Warsaw* (Polish Scientific, Warsaw, 1972), p. 1023.
[48]H. J. Lee, L. Y. Juravel, and J. C. Woolley, Phys. Rev. B 21, 659 (1980).
[49]See the first reference in Ref. 43.
[50]A.-B. Chen and A. Sher, Phys. Rev. Lett. 40, 900 (1978).
[51]A. Onton and L. M. Foster, J. Appl. Phys. 43, 5084 (1972).
[52]R. J. Nelson, N. Holonyak, Jr., and W. O. Groves, Phys. Rev. B 13, 5415 (1976).
[53]H. C. Marciniak and D. B. Wittry, J. Appl. Phys. 46, 4823 (1975).
[54]M. G. Craford, R. W. Shaw, A. H. Herzog, and W. O. Groves, J. Appl. Phys. 43, 4075 (1972), and references therein.
[55]A. Onton and R. J. Chicotka, Phys. Rev. B 4, 1847 (1971).
[56]A. M. Joullie and C. Alibert, J. Appl. Phys. 45, 5472 (1974).
[57]H. M. Macksey, N. Holonyak, Jr., R. D. Dupuis, J. C. Campbell, and G. W. Zack, J. Appl. Phys. 44, 1333 (1973).
[58]C. Alibert, G. Bordure, A. Laugier, and J. Chevallier, Phys. Rev. B 6, 1301 (1972).
[59]A. Onton, M. R. Lorenz, and W. Reuter, J. Appl. Phys. 42, 3420 (1971).
[60]A. Onton, in *Festkörperprobleme* (Frieder, Vierweg, Braunschweig, 1973), Vol. XIII, p. 59.
[61]G. D. Pitt, M. K. R. Vyas, and A. W. Mabbit, Solid State Commun. 14, 621 (1974).
[62]H. Kroemer, W-Y. Chien, J. S. Harris, Jr., and D. D. Edwall, Appl. Phys. Lett. 36, 295 (1980).
[63]G. A. Baraff and M. Schluter, Phys. Rev. B 19 (1969).
[64]J. Berholc, N. O. Lipari, and S. T. Pantelides, Phys. Rev. Lett. 41, 895 (1978).
[65]S. G. Louie, Phys. Rev. B 22, 1933 (1980).
[66]G. Dresselhaus and M. S. Dresselhaus, Phys. Rev. 160, 649 (1967).
[67]D. J. Chadi, Phys. Rev. B 16, 790 (1977).
[68]R. Dornhaus and G. Nimtz, in *Springer Tracts in Modern Physics 78*, edited by G. Höhler (Springer, Berlin, 1976), p. 1.